

The Impact of the M43 HII Region on the Orion A Molecular Cloud

Carlos E. Carrillo-Gallegos, Héctor Arce
Yale Department of Astronomy

Abstract	2
1. Introduction	3
2. Data and Observations	4
3. Analysis	5
3.1 Extent of the M43 HII Region	5
3.2 Column Density	6
3.3 Mass	7
3.4 Position-Velocity Diagrams	8
3.5 Kinetic Energy and Momentum	12
3.6 Intensity Profiles	12
4. Discussion	13
4.1 Mass Estimates and Optical Depth of ^{13}CO .	13
4.2 Comparison of Mass Estimates	14
4.3 Comparison of Kinetic Energy and Momentum Estimates	14
4.4 Intensity Profiles	16
5. Conclusions	18
6. Acknowledgements	18
7. Notes	19
8. References	19

Abstract

HII regions are among the most prominent signposts of high-mass star formation. They are formed by the ionizing photons from a newborn high-mass star. As such, they can have a physical and chemical impact on the molecular gas of their parent cloud. Messier 43 (M43), a small HII region in the Orion A molecular cloud, just north of the Orion Nebula, is significant for three reasons: it is a part of the nearest high-mass star forming region, is reasonably spherical (a useful simplification for calculating its physical properties), and is largely unstudied. A central goal of the project is to define the extent of the region of the Orion A molecular cloud that has been impacted by the HII region, and to determine the mass of the impacted region. For this, we use the ^{12}CO , ^{13}CO and C^{18}O (1-0) maps from the CARMA-NRO Orion survey. We also constructed position-velocity diagrams of the region using ^{12}CO and CII data (from SOFIA-GREAT observations) to compare the kinematics of the atomic gas with that of the molecular gas and estimate M43's expansion velocity as derived from these two different tracers. We then use the estimated mass and expansion velocity to estimate the momentum and kinetic energy that the HII region has injected into the cloud. Lastly, we study the chemical impact of the HII region on the molecular gas by comparing the abundance of various atomic and molecular species as a function of the distance from M43's exciting source. In the future, the project will extend the process developed here for similar HII regions, and compare the results of other regions to those of M43.

1. Introduction

HII regions—regions of interstellar gas where hydrogen has been ionized into HII by young, high-mass stars—are important indicators of star formation rate and intensity. These regions directly impact the molecular gas around it, made up mostly of molecular hydrogen, H₂, as it is by far the most abundant gas in the universe. The molecular gas also contains other important gasses, such as CO isotopes, CN, CS, and CII. Because H₂ itself is poorly traced in radio emissions, we use the previously mentioned gasses in our survey of the impact of HII regions on their surrounding molecular clouds.

M43 is a nebula in the Orion A Molecular Cloud, the nearest high-mass star forming region. It houses a significant HII region, the M43 HII region, which is an interesting object of study for three main reasons. First, its relatively immediate proximity (being located in Orion A), makes it a useful object via which to study HII regions—many other regions are not observable at the same level of precision. Additionally, radio continuum maps indicate that the HII region is relatively spherical (Subrahmanyan et al. 2001), a useful physical simplification that is not always applicable to astronomical objects. This simplification can prove useful when calculating some physical properties of M43. Lastly, as of yet there has been relatively little study focusing on M43. A thorough survey of the HII region will thus be mostly unique and will serve as a useful case study to determine more about the properties of HII regions in general.

In our study of M43, we aim to quantify the physical properties of the HII region and its effects on the surrounding molecular cloud. More specifically, we aim to make estimates of the region's extent, then calculate the mass of the impacted molecular gas, kinetic energy and momentum injected into the cloud. We then compare the kinetic energies and momentums obtained to other astronomical processes—in particular stellar feedback and supernovae

explosions, in order to confirm the relative accuracy of our results. We also produce intensity profiles of the region using several different tracing gasses. The majority of the analysis done is achieved through python functions we have written and packaged as an installable python package to facilitate the reproduction of the process on other HII regions. Provided ^{13}CO data cubes and DS9 region files, the code can compute estimates of column densities, mass, kinetic energy, momentum, pressures, and produce position-velocity diagrams.

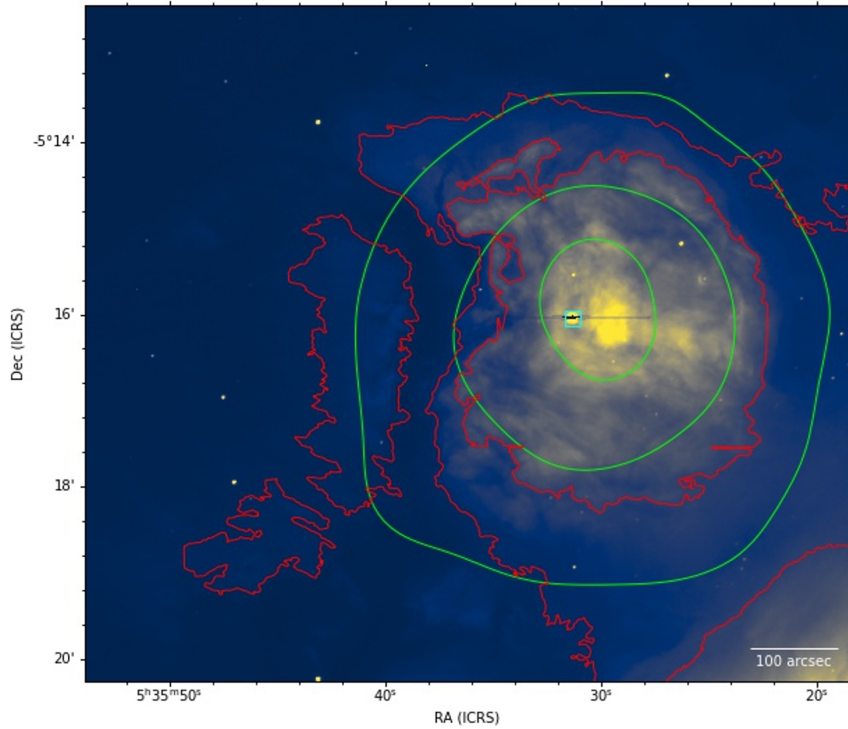


Figure 1: The M43 HII Region, shown in H-alpha. The green contours represent the radio continuum contours, the red contours represent H-alpha emission, and the cyan square shows the location of the ionizing star.

2. Data and Observations

The bulk of our analysis is completed using ^{12}CO , ^{13}CO and C^{18}O (1-0) maps from the CARMA-NRO Orion survey. We also employ CII data from the SOFIA-GREAT survey to create position-velocity diagrams, and H-alpha data. Lastly, CN and CS data is sourced from the Owens

Valley Radio Observatory. The data used are 3-D velocity cubes, meaning that at different velocities, different images are included in the dataset, indicating how much gas is present at each velocity channel.

3. Analysis

3.1 Extent of the M43 HII Region

Before computing the physical properties of M43, we define a set of possible regions to estimate the size of the HII region. Because there is no objective extent, we use two estimates in order to provide lower and upper bounds on the physical properties of the region. The objective of our region estimates is to include all of the gas the HII region is realistically capable of impacting with its expansion.

The simplest and smallest estimate is made using a contour from the radio continuum data (Subrahmanyam et al. 2001). We can safely assume that M43 is accurately resolved in the radio continuum, and so the largest contour representing that region in the data is used as our lower-bound estimate for the extent of M43.

The higher bound estimate built off of the radio continuum approximation, with adjustments to make it larger. To make these adjustments, we use excitation temperature maps (Tex) in ^{12}CO , which are a useful tool in visualizing where there is a lot of energy exchange ongoing in the region. We also utilized H-alpha emission data in making the region, as H-alpha is known to trace the boundaries of HII regions. These two factors were considered when making the larger M43 region estimate. This larger estimate for the region is potentially slightly larger than realistic, but provides a useful upper limit for the region. The two estimates are pictured

over an integrated-intensity map in Figure 2. Going forward, all physical properties will be computed on both regions.

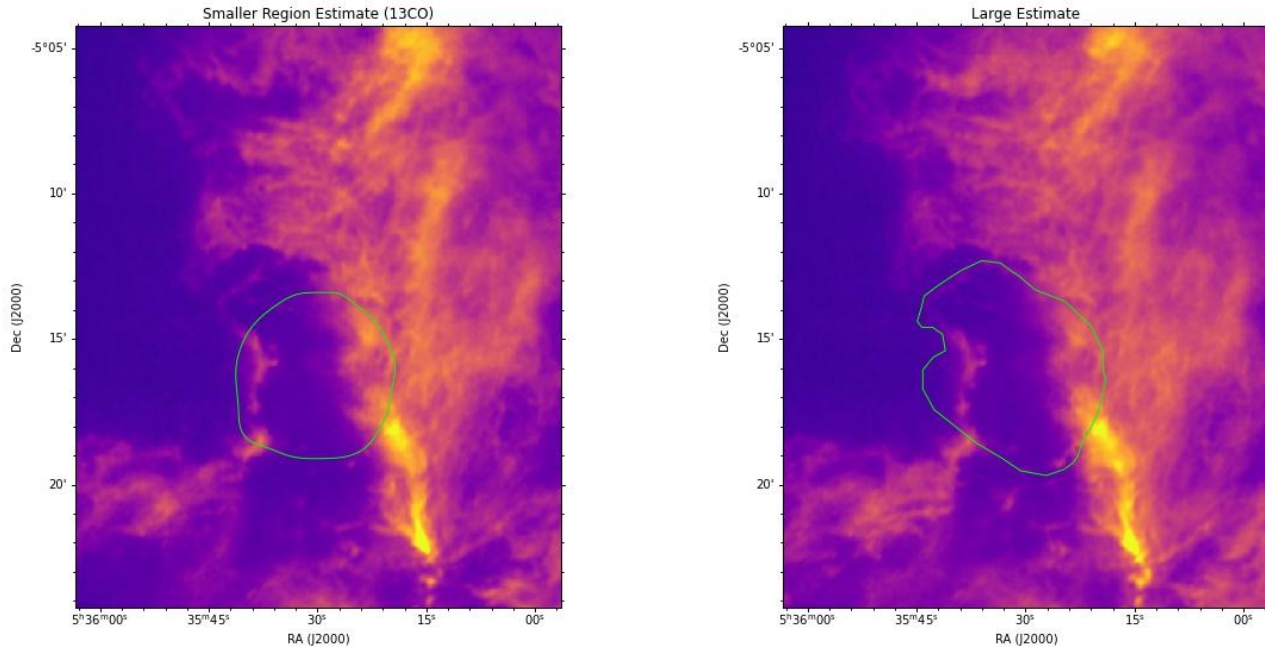


Figure 2: The smaller region is overlaid in green on the left, and the larger region is in green on the right. Both are on top of an Integrated Intensity Map of M43 in ^{13}CO

3.2 Column Density

In order to estimate the mass of the impacted gas, we must be able to determine its column density in H_2 . Column density is a measure of the number of molecules in the line of sight of a pixel in an astronomical image. There are various different methods for computing column density, all dependent on the tracing gas being used to compute it.

In this study, we use the approach from Pineda et. al 2008 on ^{13}CO tracing gas. We use ^{13}CO as our estimation method, as ^{12}CO is known to be optically thick in this region, which would make accurate estimation of column density much more difficult. ^{13}CO is certainly less optically thick than ^{12}CO , but not assuredly optically thin. For that reason, we make two

estimations of the column density for each region estimate: one assuming that ^{13}CO is optically thin, and one assuming that it is optically thick.

$$\tau(^{13}\text{CO}) = -\ln \left[1 - \frac{T_{\text{max}}(^{13}\text{CO})/5.3 \text{ K}}{1/(e^{5.3 \text{ K}/T_{\text{ex}}} - 1) - 0.16} \right]$$

Equation 1: The optical depth equation for ^{13}CO

In the optically thick limit, we use equations 7 and 9 from Pineda exactly as they are provided. In the optically thin limit, we remove the optical depth correction factor in equation 9. If the mass estimates we obtain vary significantly based on the two different methods, then we know that the cloud is not optically thin, and that the correction factor is needed.

$$N(^{13}\text{CO}) = \left[\frac{\tau(^{13}\text{CO})}{1 - e^{-\tau(^{13}\text{CO})}} \right] 3.0 \times 10^{14} \frac{W(^{13}\text{CO})}{1 - e^{-5.3/T_{\text{ex}}}} \text{ cm}^{-2}$$

Equation 2: The column density equation for ^{13}CO , where $W(^{13}\text{CO})$ is the integrated intensity and the bracketed term is the optical depth correction.

To compute the column densities, we required three different data maps. First, an integrated intensity map in ^{13}CO which summed up all significant emission from the original data cube. Second, an excitation temperature map—the same one used in our estimate of the region’s extent. Although the excitation temperature map is made using ^{12}CO data, it still functions properly with the ^{13}CO column density. Lastly, for the optically thick limit in which we need to compute the optical depth of the region, we made a maximum temperature map, which took the highest values in the ^{13}CO data cube at each pixel to create one two-dimensional map.

3.3 Mass

In order to compute the mass of the region, we masked the column density maps with the regions described in 3.1. From there, we computed the mass in each pixel, multiplying the masked column density map by the area of each pixel ($1 \times 10^{44} \text{ cm}^2$) and the mass of a single

molecule of H₂ (4.5×10^{-27} kg). Because we are interested in the mass of the region in H₂, and our column densities are computed using ¹³CO data, we multiply by a conversion factor (7×10^5), which is an estimated ratio of how many H₂ molecules are present for every ¹³CO molecule. After that, we sum up the mass of all the pixels which gives us the mass estimate for the M43 HII region.

The results are detailed in Table 1. In the not optically thin limit, we note that our estimates yielded results between 660 and 760 M _⊕. In the optically thin limit, we estimated approximately 570-660 M _⊕.

3.4 Position-Velocity Diagrams

Given the mass, we now have one-half of the physical properties needed to compute the system's kinetic energy and momentum, which are the most important aspects in quantifying the impact of M43 on its surrounding molecular cloud. We must now find an estimate of the expansion velocity of the region.

To do this, we made position-velocity diagrams, which collapse the data cube into a 2-dimensional image, with position (offset from the starting point of the line) on the x-axis, and velocity on the y-axis. We made several different diagrams representing several different cuts along the region, collapsing along both the right-ascension and the declination axis. We made these diagrams using CII and ¹²CO data.

The expansion velocity can be determined from a position-velocity diagram if there is a clear offset from the base velocity at some point in the diagram. It was expected that CII would clearly show the expansion velocity in at least some cuts of the region (Pabst et. al 2020), but we did not have expectations for ¹²CO.

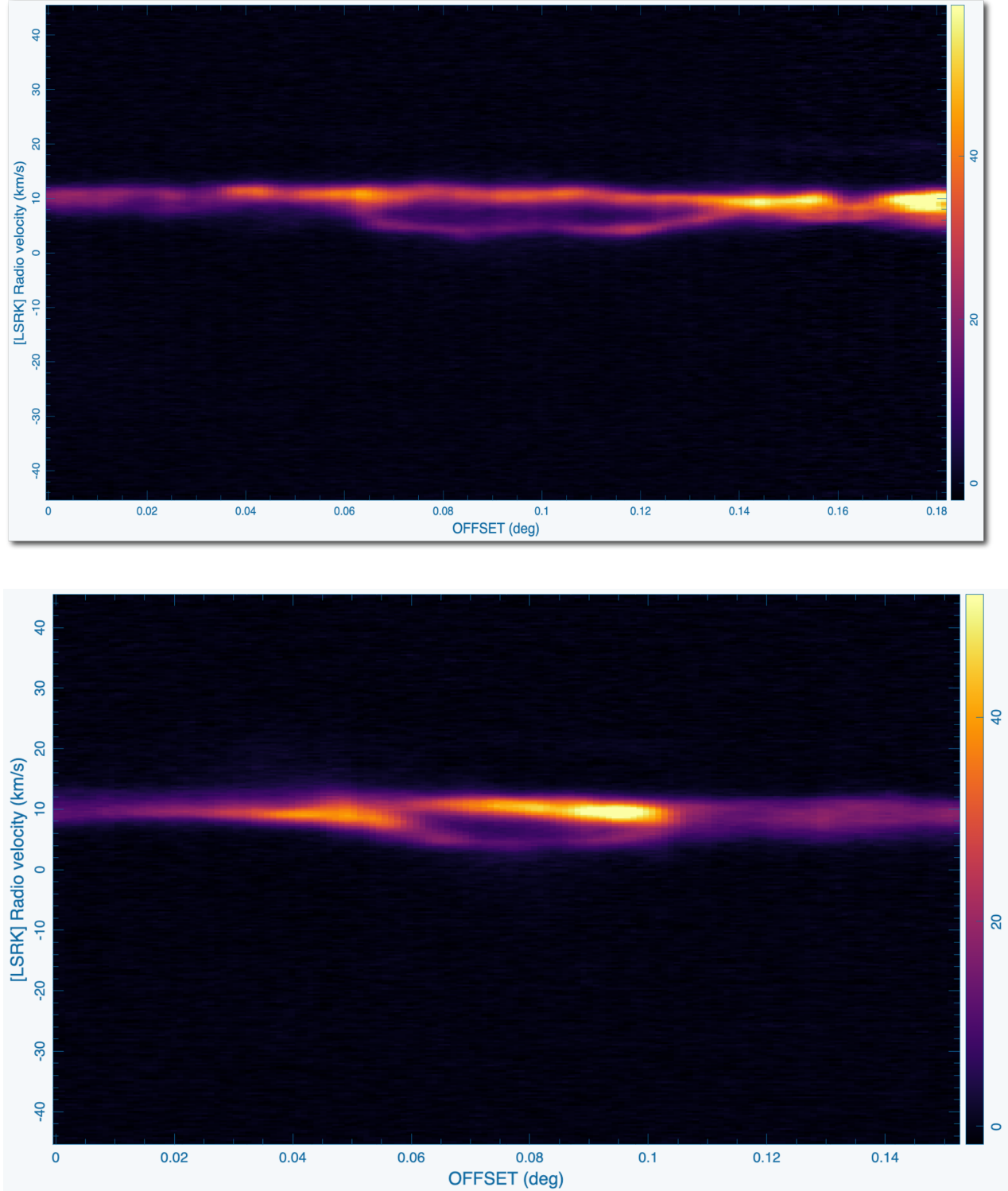


Figure 3: Position-Velocity Diagrams in CII. The top plot represents a vertical cut through the region, and the bottom plot represents a horizontal cut. The clear deviation from the standard velocity indicates a clear expansion velocity of 6 km/s.

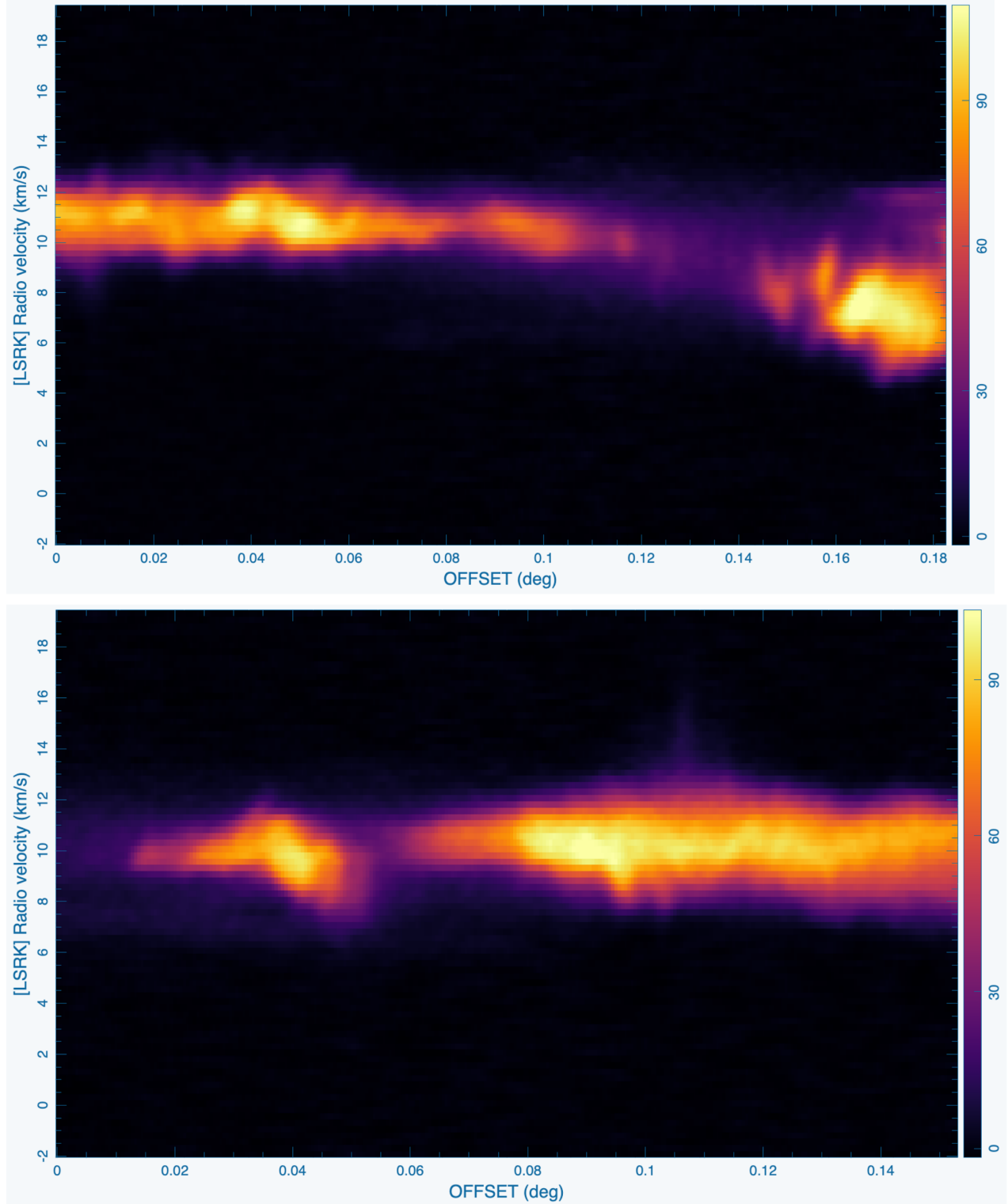


Figure 4: Position-Velocity Diagrams in ^{12}CO . The top plot represents a vertical cut through the region, and the bottom plot a horizontal cut. The lack of clear bubbles deviating from the standard velocity means we cannot determine the expansion velocity of the cloud using ^{12}CO .

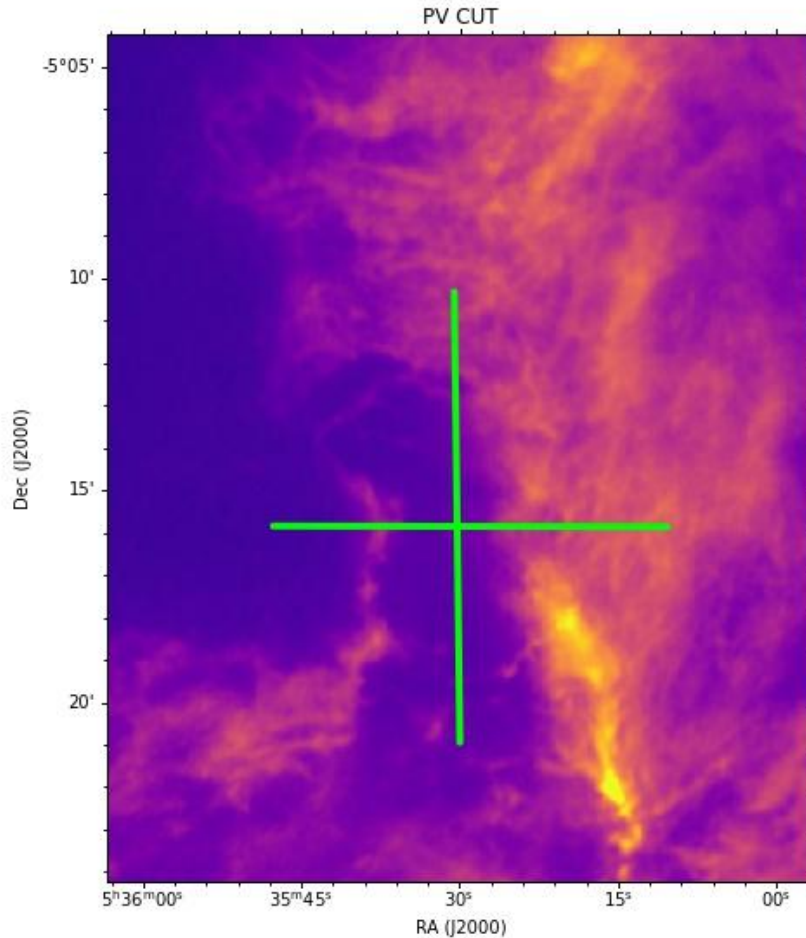


Figure 5: The horizontal and vertical cuts along which the pictured position-velocity diagrams were made. Several other cuts were used spanning the whole region—these two cuts returned the best values in CII.

Ultimately, the ^{12}CO data did not indicate any expansion velocity, but the CII data showed expansion velocity of about 6 km/s in several cuts. Similar analysis with CII and ^{12}CO data was done by Pabst et. al 2020 yielding the same results (or lack of results in ^{12}CO). We thus use that value as our expansion velocity in our estimation of kinetic energy and momentum. Some position-velocity diagrams are pictured above in Figures 3-4.

3.5 Kinetic Energy and Momentum

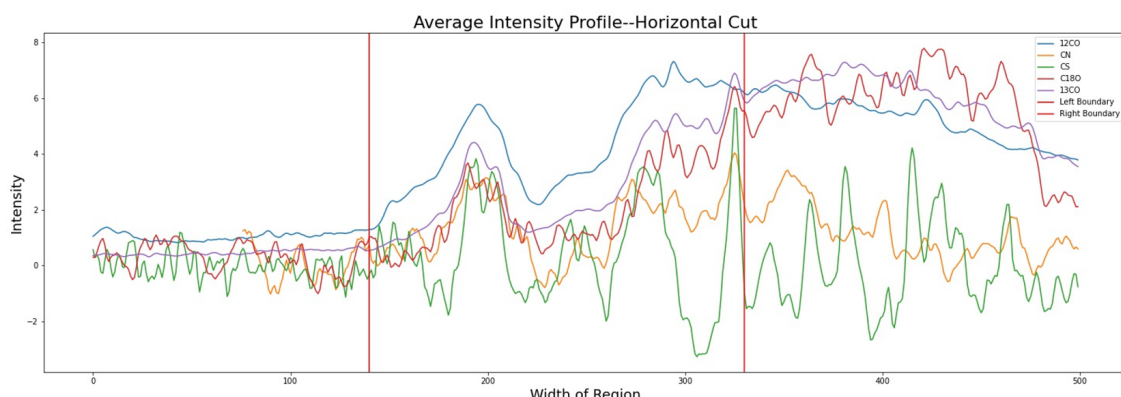
The kinetic energy and momentum are computed using the standard equations: mass times velocity for momentum, and $\frac{1}{2}$ mass times velocity squared for kinetic energy. The results are shown in Table 1. The accuracy of our results is assessed in section 4.2 by comparing the values obtained to those of supernovae as an upper bound and stellar outflows as a lower bound.

Column Density Estimate	Mass (Solar Masses)	Momentum (Solar Masses* km/s)	Kinetic Energy (Ergs)
Not Optically Thin	$6.60 \times 10^2 - 7.60 \times 10^2$	$4.0 \times 10^3 - 4.5 \times 10^3$	$2.3 \times 10^{47} - 2.7 \times 10^{47}$
Optically Thin	$5.70 \times 10^2 - 6.60 \times 10^2$	$3.5 \times 10^3 - 4.0 \times 10^3$	$2.0 \times 10^{47} - 2.4 \times 10^{47}$

Table 1: Mass, Momentum, and Kinetic Energy of the gas impacted by the M43 HII Region.

3.6 Intensity Profiles

In addition to computing the physical aspects of M43, we also look at the intensity profiles of 5 five different tracing gasses: ^{12}CO , ^{13}CO , C^{18}O , CN, and CS. We look with particular interest at the behavior of the gasses near what we expect to be the boundaries of the HII region, to see how effectively they trace HII regions. These profiles are taken with horizontal and vertical cuts through the region, averaged over a width of approximately 10 pixels. They are pictured in Figure 6 and discussed in section 4.4.



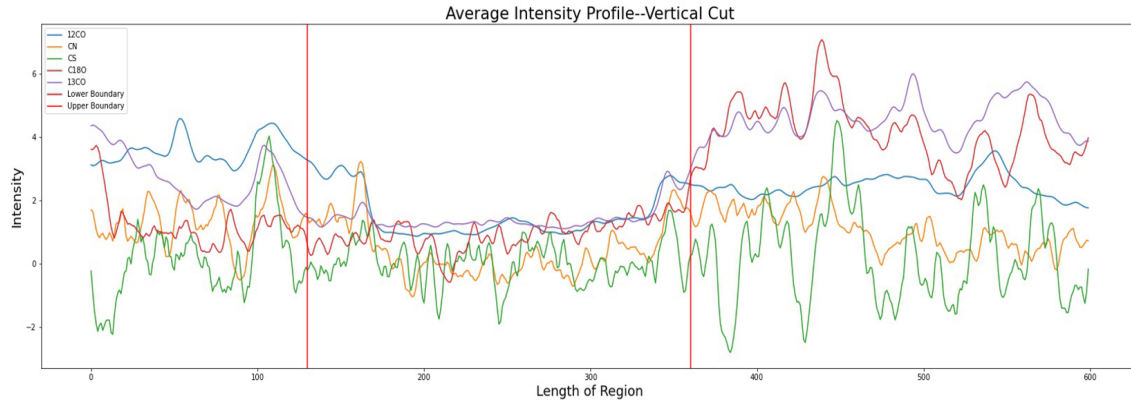


Figure 6: Intensity profiles of M43 in several different tracing gasses. **Top:** Horizontal cut through the region. **Bottom:** Vertical cut through the region. X-axis for both plots in pixels, y-axis in scaled intensity. Profiles for ^{12}CO , ^{13}CO , C^{18}O scaled to fit on same plot as CN, CS

4. Discussion

Here, we discuss the accuracy of our mass estimates and make a determination as to the optical depth of ^{13}CO being impacted by M43. We also compare the quantities we've obtained for mass, kinetic energy, and momentum with other astronomical phenomena in order to determine the plausibility of our estimates. We also discuss the intensity profiles and whether any significant information can be gleaned from them.

4.1 Mass Estimates and Optical Depth of ^{13}CO .

Given that we obtained two distinct mass estimates depending on whether or not we assumed ^{13}CO was optically thin, it can be reasonably assumed that the ^{13}CO gas does not adhere to the optically thin limit. Had the two results been nearly identical, it would indicate that the optical depth correction factor in the column density calculation was not accounting for much, and thus the gas could be assumed optically thin. Note that the gas not being optically thin does

not mean it is optically thick—that would not be a reasonable assumption for this gas either. It simply indicates that the gas is neither optically thin nor thick.

4.2 Comparison of Mass Estimates

To ensure the plausibility of our mass estimate at approximately $660\text{-}760 M_{\odot}$, we compare our result to an estimate for the mass of a large portion of the Orion A Molecular Cloud (Figure X). Kong et al. 2018 estimated the mass of this region to be approximately $10^5 M_{\odot}$. Our estimates for the extent of M43 are overlaid in green on the figure. Thinking proportionally, it is entirely reasonable that a region only as large as M43 could contain approximately 0.7% of the mass of the entire area. This is not a thorough analysis, of course, and does not account for differences in density that definitely exist throughout the region, but it assures us that our results are plausible.

4.3 Comparison of Kinetic Energy and Momentum Estimates

In order to assess the plausibility of our estimates for kinetic energy and momentum, we compare the results here with other astronomical phenomena. On the lower end of the spectrum, we compare the kinetic energy and momentum imparted by M43 with that coming from stellar outflows. We expect stellar outflows to be less energetic. On the other hand, we also compare our values to the kinetic energy and momentum associated with a supernova explosion, which we expect to be very energy intensive and far more significant than the values observed for M43.

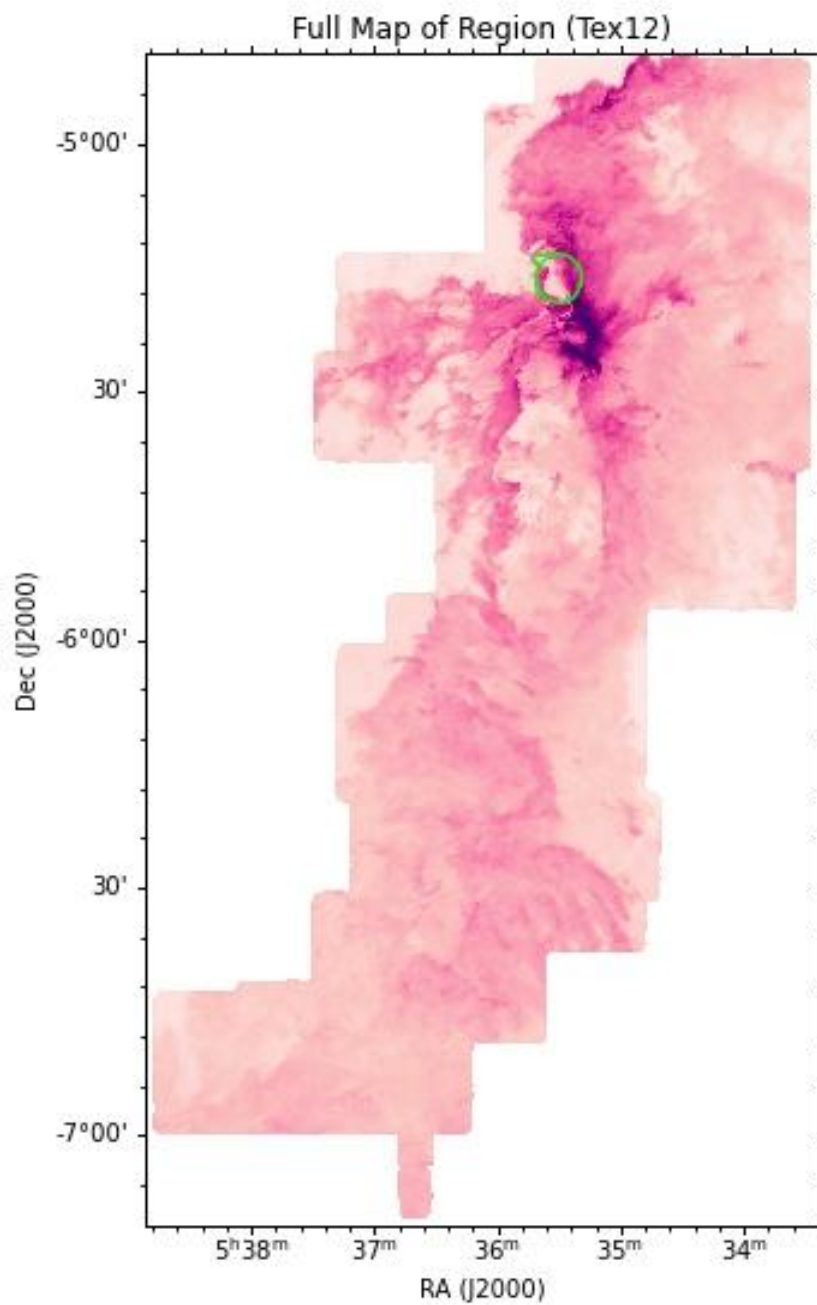


Figure 8: Map of a large portion of the Orion A Molecular Cloud, with the approximate extent of M43 in green. The map is of the excitation temperature in ^{12}CO (Tex12), which helps identify regions of significant activity. Tex map from Kong et. al 2018

We obtain estimates for the kinetic energy and momentum of a set of stellar outflows from Feddersen et. al 2020, which looked at the summed values of several stellar outflows in the Orion Molecular Cloud. Our values for supernova explosions are obtained via Walch et. al 2015, where they simulated supernova activity. We use estimates for kinetic energy and momentum that they used to conduct their simulations. The comparisons are laid out in Table 2.

Source	Momentum (Solar Mass x km/s)	Kinetic Energy (ergs)
Stellar Outflows <small>Feddersen et al., <i>Astrophysical Journal</i> 2018</small>	50-200	2.0×10^{45} - 6.0×10^{45}
M43 HII Region	4.0×10^3 - 4.5×10^3	2.3×10^{47} - 2.7×10^{47}
Supernovae <small>Walch et. Al., <i>Royal Astronomical Society</i> 2015</small>	2.8×10^4	$\sim 10^{51}$

Table 2: Comparison of Kinetic Energy and Momentum

We find that the values for M43 fall exactly in line as we expect—higher than stellar outflows and lower than supernova explosions. This gives credence to our results being realistic for the energy and momentum injected by the HII region on its surrounding cloud.

4.4 Intensity Profiles

The lower and upper boundaries indicated on the intensity profiles are determined by the furthest extent of our largest estimate for the M43 HII region. This serves two purposes. First, it provides generous upper and lower bounds for our profiles—any activity happening beyond these bounds are almost certain to be separate from the impact of M43 because we defined the large

region to be generously large. Secondly, the profiles can help us determine whether or not our bounds are reasonably accurate.

The most significant feature, most notable in the horizontal cut, is that all the gasses' profiles behave in the way we would expect. As seen in Figure X, the integrated intensity map of M43, there is a cavity near the center of the region where there is very little molecular gas. This is identifiable in the profiles between the 200th and 300th pixels, in between which there is a peak in emission, a significant dip, and another spike, indicating the presence of a cavity. This is to be expected; as a young, high-mass star evolves, it ionizes the gas nearest to it and little molecular gas remains in the center of the region.

As for using the profiles to evaluate the accuracy of our large region estimate, we see that all five gasses except ^{12}CO begin peaking well inside of the left boundary in the horizontal cut, indicating that perhaps a more accurate boundary would be closer than it currently is. Looking at the vertical cut, we see again that all gasses except for ^{12}CO have a local peak decently inside of the lower boundary. This is not unexpected, as we made the region intentionally large, but we should also note that the differences between the molecular-gasless cavity and the boundary of the region are not as pronounced along Right Ascension as they are about Declination. That is to say, in the x-axis the limits of the cavity are clear, and as such the profiles are largely predictable. The same does not apply in the y-axis cuts of the region.

On the right boundary in the horizontal cut, however, we note that again all gasses except ^{12}CO have a sharp peak right before the right boundary definition. If the right boundary is accurate, which is not an unreasonable assumption as the rightmost side of the large region estimate is almost identical to that of the small estimate (because there is less ambiguity about how far the impacted gas extends), then this could indicate that CN and CS (as well as ^{13}CO and

C^{18}O) trace HII regions extremely closely. This is not an official conclusion that can be derived from this study, of course, as the level of analysis of these profiles is not sufficient to make such direct claims. However, it does point to an interesting avenue of further study.

5. Conclusions

The most significant result of this study has been the accurate quantification of the impact of the M43 HII region on its surrounding molecular gas. While other papers have contributed to the understanding of M43, this paper provides a more thorough focus on the region and computes its mass, kinetic energy, and momentum. Given our improved understanding of M43, it can be used as an effective case study for other HII regions for which such a detailed analysis is not possible (perhaps HII regions in other galaxies, for example).

Additionally, this paper also provides a framework for future study of other HII regions. The quantification of other impacted regions of molecular gas is straightforward given the process outlined in this paper. Furthermore, the python code used to conduct this analysis has been packaged into an installable python package extendable to any other HII region, provided proper data and region file availability.

Finally, this study also raises an interesting question related to CN, CS, and how well they trace HII regions. Further studies of how these two tracing gasses in particular interact with HII regions would illuminate our understanding of how closely gasses trace these regions, and improve our ability to better define HII regions in the future.

6. Acknowledgements

This study would not have been possible without the generous support of the Yale STARS II program, which funded some of this research, and the Yale Summer Experience

Award, which funded the rest of the study. The authors are also indebted to the Yale Department of Astronomy for their support.

7. Notes

The code used for the majority of this analysis has been packaged into a python package found here: <https://github.com/CarlosECarrilloGallegos/h2reg>

8. References

- Feddersen, J. R., Arce, H. G., Kong, S., Suri, S., Sánchez-Monge, Á., Ossenkopf-Okada, V., Dunham, M. M., Nakamura, F., Shimajiri, Y., & Bally, J. (2020). The carma–NRO orion survey: Protostellar outflows, Energetics, and Filamentary Alignment. *The Astrophysical Journal*, 896(1), 11. <https://doi.org/10.3847/1538-4357/ab86a9>
- Kong, S., Arce, H. G., Feddersen, J. R., Carpenter, J. M., Nakamura, F., Shimajiri, Y., Isella, A., Ossenkopf-Okada, V., Sargent, A. I., Sánchez-Monge, Á., Suri, S. T., Kauffmann, J., Pillai, T., Pineda, J. E., Koda, J., Bally, J., Lis, D. C., Padoan, P., Klessen, R., ... Tanabe, Y. (2018). The Carma-NRO Orion Survey. *The Astrophysical Journal Supplement Series*, 236(2), 25. <https://doi.org/10.3847/1538-4365/aabafc>
- Pabst, C. H., Goicoechea, J. R., Teyssier, D., Berné, O., Higgins, R. D., Chambers, E. T., Kabanovic, S., Güsten, R., Stutzki, J., & Tielens, A. G. (2020). Expanding bubbles in Orion A: [C ii] observations of M 42, M 43, and NGC 1977. *Astronomy & Astrophysics*, 639. <https://doi.org/10.1051/0004-6361/202037560>
- Pineda, J. E., Caselli, P., & Goodman, A. A. (2008). CO isotopologues in the Perseus Molecular Cloud Complex: The X-factor and regional variations. *The Astrophysical Journal*, 679(1), 481–496. <https://doi.org/10.1086/586883>
- Subrahmanyam, R., Goss, W. M., & Malin, D. F. (2001). Radio Continuum Structure of the orion nebula. *The Astronomical Journal*, 121(1), 399–407. <https://doi.org/10.1086/318017>
- Walch, S., & Naab, T. (2015). The energy and momentum input of supernova explosions in structured and ionized molecular clouds. *Monthly Notices of the Royal Astronomical Society*, 451(3), 2757–2771. <https://doi.org/10.1093/mnras/stv1155>